p-State Luminescence in CdSe Nanoplatelets: Role of Lateral Confinement and a Longitudinal Optical Phonon Bottleneck

Alexander W. Achtstein,[1,*] Riccardo Scott,[1] Sebastian Kickhöfel,[1] Stefan T. Jagsch,[2] Sotirios Christodoulou,[3,4] Guillaume H. V. Bertrand,[4] Anatol V. Prudnikau,[5] Artsiom Antanovich,[5] Mikhail Artemyev,[5] Iwan Moreels,[4] Andrei Schliwa,[2] and Ulrike Woggon[1]

[1]*Institute of Optics and Atomic Physics, Technical University of Berlin, Strasse des 17. Juni 135, 10623 Berlin, Germany*
[2]*Institute of Solid State Physics, Technical University of Berlin, Strasse des 17. Juni 135, 10623 Berlin, Germany*
[3]*Department of Physics, University of Genoa, via Dodecaneso 33, IT-16146 Genova, Italy*
[4]*Istituto Italiano di Tecnologia, Via Morego 30, IT-16163 Genova, Italy*
[5]*Institute for Physico-Chemical Problems, Belarusian State University, 220030 Minsk, Belarus*

(Received 1 June 2015; revised manuscript received 18 January 2016; published 18 March 2016)

We evidence excited state emission from *p* states well below ground state saturation in CdSe nanoplatelets. Size-dependent exciton ground and excited state energies and population dynamics are determined by four independent methods: time-resolved PL, time-integrated PL, rate equation modeling, and Hartree renormalized $\mathbf{k}\cdot\mathbf{p}$ calculations—all in very good agreement. The ground state–excited state energy spacing strongly increases with the lateral platelet quantization. Depending on its detuning to the LO phonon energy, the PL decay of CdSe platelets is governed by a size tunable LO phonon bottleneck, related to the low exciton-phonon coupling, very large oscillator strength, and energy spacing of both states. This is, for instance, ideal to tune lasing properties. CdSe platelets are perfectly suited to control the exciton-phonon interaction by changing their lateral size while the optical transition energy is determined by their thickness.

DOI: 10.1103/PhysRevLett.116.116802

Semiconductor nanoparticles have attracted growing attention in the past decade due to their promising optical and electronic properties. Two-dimensional II-VI semiconductor nanoplatelets (NPLs) gained increasing interest because of their unique electronic and optical properties [1], such as the giant oscillator strength effect [2–4], room temperature exciton coherence [5] and lasing [6], strong electroabsorption response [7], and size-dependent dark-bright splitting [8]. The unusually small coupling to phonons [3] makes NPLs potential candidates for materials with low dephasing rates, high lateral conductivity, and control of both internal relaxation and energy transfer efficiencies. In this Letter we introduce a scheme for a well-defined control of exciton-phonon interaction by lateral size variation. Efficient *p*-state luminescence is observed in CdSe NPLs and their energies confirmed by theory. Tuning the *s*-*p* energy separation allows us to suppress or enhance the coupling to LO phonons paving the way to a controlled switching of energy relaxation, charge transport, or resonant energy transfer by lateral NPL size control. For the investigated CdSe NPLs, Fig. 1(a) shows the evolution of the lowest exciton *s* and *p* states with increasing transversal confinement and anisotropy, and Fig. 1(b) shows their wave functions and allowed transitions.

We show in this Letter that the ground state–excited state energy difference of CdSe NPLs strongly increases with the lateral platelet quantization and that the observed biexponential photoluminescence (PL) decay of NPLs is connected to the very large radiative rates of the excited state (ES) and ground state (GS) and a phonon bottleneck suppressing interrelaxation. The strong transversal confinement-related suppression of LO phonon modes in the NPLs

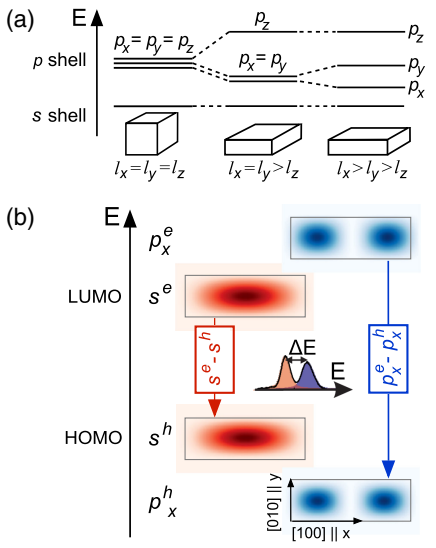

FIG. 1. (a) Evolution of the electron *p*-shell degeneracy when an isotropic quantum box evolves into a platelet with unequal side lengths. (b) Overview of the allowed optical transitions observed in experiment along with wave function probability density plots in real space and an observed ground state (GS) and excited state (ES) PL spectrum.

[3], also identified as lifetime limited dephasing rates [4], results here in a slowdown of the ES-GS exciton transfer rate and subsequent visible ES luminescence well below ground state saturation.

Figure 2 shows the photoluminescence spectra of the investigated 4.5 monolayer (ML) CdSe NPLs embedded in PMAO films on thin fused silica substrates and mounted in a liquid He cryostat [synthesis, TEM characterization, experimental conditions; see Supplemental Material [9]]. The dual emission peaks observed in the time-integrated spectra of Fig. 2(a) are assigned to the *s*- and *p*-type ground and excited state emission of CdSe NPLs. Voigt fits are used to determine the peak centers and the integrated peak area ratios of the ES and GS as plotted in Fig. 2(b) versus the ES-GS energy difference ΔE. Surprisingly, a clear minimum close to 25.4 meV is observed as a first hint to lateral confinement controlled LO-phonon coupling. From Fig. 2(c) it can be seen that the energy difference ΔE increases from 18 to 38 meV with increasing lateral platelet confinement. We thus exclude that this energy spacing is related to a zero-phonon peak and its first LO phonon replica (as, by chance, inferred in Ref. [8]), as it should have a nearly confinement-independent energy spacing of the LO phonon energy 25.4 meV [24] and the same dynamics as the zero-phonon line. Biexciton and trion emission and GS saturation can be ruled out by cw and power-dependent measurements as given in the SM along with a table listing the experimental energy spacings [9]. To support the hypothesis of *p*-state emission and control of LO-phonon coupling by lateral size, we investigate the luminescence dynamics of both emissions as shown in Fig. 3 by streak camera measurements on two time scales.

Figures 3(a) and 3(b) display a PL transient of 29×8 nm^2 (lateral dimensions) platelets along with spectral cuts in time showing the evolution of the dual ES-GS emission. A fast ES and a slower GS PL decay can be observed and separated by fitting the spectral contributions versus time [Fig. 3(b)]. The ES fills the GS, while the ground state decays then on a longer time scale. Depending on the detuning ($\Delta E_{\text{ES-GS}} - E_{\text{LO}}$) of the ES-GS energy spacing from the LO phonon energy in different samples [Figs. 3(c)–3(f)], we observe in resonance to the LO phonon energy an ultrafast ES recombination and GS filling, whereas in the case of off resonance the ES dynamics is much slower. This effect is directly related to the existence of an ES-GS LO phonon bottleneck which suppresses the ES-GS interrelaxation in the case of off resonance. Correspondingly, an increase of the ES/GS emission intensity ratio with increasing detuning from the minimum at the LO phonon resonance of 25.4 meV [24] is seen in Fig. 2(b). This trend is independently confirmed both by the time-integrated ES/GS intensity ratios deduced

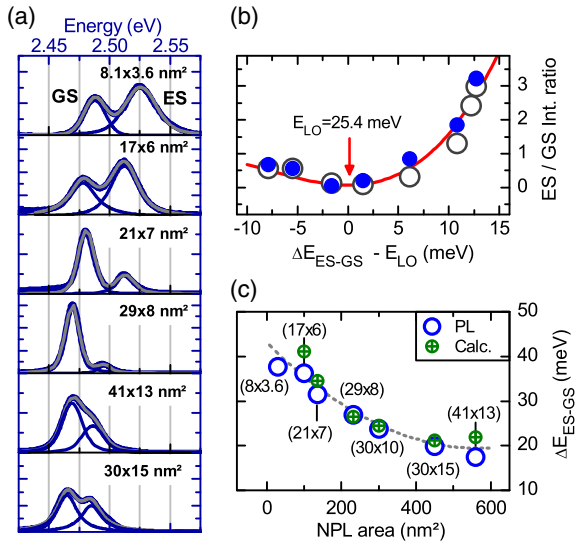

FIG. 2. (a) Time-integrated PL emission of 4.5 monolayer (ML) CdSe NPLs with increasing lateral size from top to bottom at 4 K (blue lines). Excitation at 420 nm and ~0.2 W/cm^2 by a 150 fs 75.4 MHz Ti:sapphire laser (as in all other measurements). The GS and ES emission peaks are fitted with Voigt profiles. (b) LO phonon bottleneck. ES-GS PL intensity ratios at 4 K deduced from (a) (open dots) and from time-resolved spectra (Fig. 3) $(A_1^{\text{ES}}\lambda_F^{-1} + A_2^{\text{ES}}\lambda_S^{-1})/(A_1^{\text{GS}}\lambda_F^{-1} + A_2^{\text{GS}}\lambda_S^{-1})$ as reasoned from rate equation model (solid dots) versus the detuning of the ES-GS energy spacing $\Delta E_{\text{ES-GS}}$ to the LO phonon energy. (c) $\Delta E_{\text{ES-GS}}$ from experiment (circles) and our calculations (crossed dots) plotted versus the CdSe NPLs' area (sizes in nm in parenthesis, dotted line only a guide to the eye).

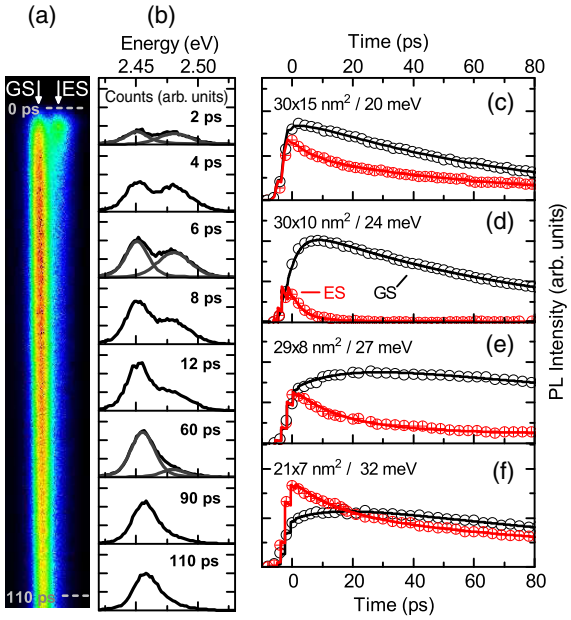

FIG. 3. (a) Transient PL decay and evolution of the ES and GS emission with time and (b) exemplary Voigt fits for a platelet size of 29×8 nm^2. (c)–(f) ES (red) and GS (black) transients obtained from Voigt fits as in (b) for different NPL sizes and $\Delta E_{\text{ES-GS}}$ for 2 ps temporal bins at 4 K. Fits to rate equation model (solid lines) include convolution with the instrument response.

from biexponential fits (to be reasoned later) to the ES and GS decay transients [Figs. 3(c)–3(f)] and from the non-time-resolved PL data in Fig. 2(a).

At elevated temperatures the method of spectral ES-GS separation as shown in Fig. 3 is impossible due to an increased homogeneous line broadening. For the analysis of the temperature-dependent dynamics, we therefore use the spectrally binned PL decay transients shown in Fig. 4 [for 29×8 nm^2 4.5 ML NPLs in the fast [4(a)] and slow [4(b)] time range at different temperatures and for 41×13 nm^2 platelets in Figs. 4(c) and 4(d)]. To avoid fitting ambiguities, the PL transients in the fast time range

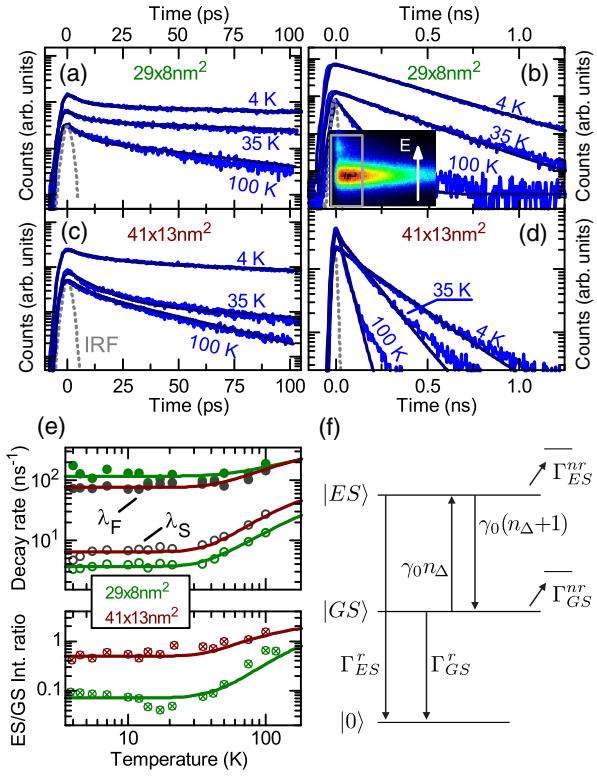

FIG. 4. (a)–(d) Blue lines: Representative examples of PL decay curves at 4, 35, and 100 K of CdSe NPLs with lateral size of 29×8 nm^2 (a),(b) and 41×13 nm^2 (c),(d). The biexponential fits (on top of data) to the fast time range decays (a),(c) use the long decay time derived from monoexponential fits to the curves in (b) and (d) recorded in a wider time window. The instrument response function (gray line) is used for deconvolution. Inset: Spectrally dispersed streak camera image of the PL decay in the first 0.5 ns of 29×8 nm^2 CdSe NPLs at 4 K. Excited state emission is clearly visible. The time range of (a) is indicated by a gray frame. (e) Decay rates of 29×8 and 41×13 nm^2 NPLs from time-resolved PL measurements (top panel) and time-integrated ES/GS PL intensity ratios (lower panel) versus temperature. The ES-GS energy spacing $\Delta E_{\text{ES-GS}}$ was held fixed when simultaneously fitting Eq. (S3) (in SM [9]) to the fast and slow decay rates, λ_F and λ_S, and Eq. (S6) (in SM [9]) to the intensity ratios (solid lines). (f) Energy level scheme used for our rate equation model.

are fitted with biexponential PL decays [$I = A_1 \exp(-\lambda_F t) + A_2 \exp(-\lambda_S t)$], using the slow rate λ_S obtained from a monoexponential fit to the long time range PL decay as fixed parameter. This procedure is reasoned via an analytical solution of a rate equation model depicted in Fig. 4(f) for the $|\text{ES}\rangle$ (p state), $|\text{GS}\rangle$ (s state), and vacuum state $|0\rangle$:

$$\dot{n}_{\text{ES}} = -n_{\text{ES}}[\Gamma^r_{\text{ES}} + \Gamma^{nr}_{\text{ES}} + \gamma_0(n_\Delta + 1)] + n_{\text{GS}}\gamma_0 n_\Delta,$$
$$\dot{n}_{\text{GS}} = -n_{\text{GS}}(\Gamma^r_{\text{GS}} + \Gamma^{nr}_{\text{GS}} + \gamma_0 n_\Delta) + n_{\text{ES}}\gamma_0(n_\Delta + 1),$$

with n_i ($i = \text{ES}, \text{GS}$) the state population, $\Gamma^{r,nr}_i$ its radiative and nonradiative decay rates, and $\gamma_0 n_\Delta$ the thermally activated (GS → ES) and $\gamma_0(n_\Delta + 1)$ the (ES → GS) scattering and relaxation rates [8,25]. $n_\Delta = 1/(e^{\Delta E/k_B T} - 1)$ is the Bose-Einstein phonon occupation factor for the energy spacing ΔE. The nonradiative rate is assumed to be a thermally activated process according to $\Gamma^{nr}_i = \Gamma^{nr,0}_i e^{-\Delta E^t_i/k_B T}$, with a trapping frequency factor $\Gamma^{nr,0}_i$ and an activation energy ΔE^t_i, assumed to be identical for ES and GS [Fig. 4(f)]. The analytical solutions to this rate equation system are biexponentials for both ES and GS with different decay amplitudes but sharing the same slow and fast decay rates, λ_S and λ_F. The time-integrated PL intensity ratio of ES and GS can be expressed with the same set of parameters. Using the results of biexponential PL decay fits [Figs. 4(a)–4(d)] we globally fit the temperature dependence of the fast and slow decay rates together with the time-integrated ES/GS emission ratios in Fig. 4(e) with our rate equation model. In order to further reduce fitting ambiguities, the experimental energy spacings ΔE from Fig. 2(a) are held fixed. Details on the rate equation model are provided in the SM [9]. Figure 4(e) shows the excellent agreement of our fit with the experimental fast and slow decay rates and PL emission intensity ratio for the 29×8 and 41×13 nm^2 samples. We obtain for the intrinsic radiative rates of the 29×8 nm^2 NPLs ($\Gamma^r_{\text{ES}} = 16$ ns^{-1}, $\Gamma^r_{\text{GS}} = 3.7$ ns^{-1}, $\gamma_0 = 101$ ns^{-1}) and for the 41×13 nm^2 NPLs ($\Gamma^r_{\text{ES}} = 50$ ns^{-1}, $\Gamma^r_{\text{GS}} = 6.4$ ns^{-1}, $\gamma_0 = 25$ ns^{-1}). With increasing lateral platelet size, the ES and GS PL decay tends to become faster (higher rates) in line with the predictions of the giant oscillator strength effect [26]. Further, we observe very large ES radiative rates enabling us to observe dual ES and GS PL emission. This finding is accompanied by an LO phonon mediated ES↔GS scattering rate γ_0, which is higher in the near resonant case ($\Delta E_{\text{ES-GS}} - E_{\text{LO}} = 1.5$ meV) and slows down in the off-resonant case ($\Delta E_{\text{ES-GS}} - E_{\text{LO}} = -7.9$ meV). Therefore, we have further clear evidence for the existence of a lateral size and with it an ES-GS energy-spacing-dependent LO phonon bottleneck in CdSe nanoplates. The rate equation system independently confirms the manifestation of an LO phonon bottleneck deduced from the ES/GS intensity ratios in Fig. 2(b).

Our rate model is further substantiated as it matches the measured quantum yield at 300 K (for nonradiative rates and trap state activation energies; see SM [9]).

The existence and observability of this bottleneck in CdSe nanoplates is related to the strong transversal confinement-induced reduction of density of states of energetically matching LO phonon modes [3]. This results here in a slowdown of the ES-GS exciton transfer rate. Because of this LO phonon bottleneck, it is possible to observe the ES emission even in cw PL (see also SM [9]), in contrast to conventional CdSe nanocrystals.

In the following, we will compare our experimental ES-GS energy differences with theoretical calculations. The observed increase of the ES-GS energy spacing with confinement [Fig. 2(c)] is expected for a strongly confined system [27,28].

Our samples have different lateral sizes in the l_x and l_y direction and a much smaller thickness l_z. For such structures, excited states (p states), energetically well separated from the ground state, are expected. Figure 1(a) shows the evolution of the electron p shell as the level of structural anisotropy increases up to $l_x > l_y > l_z$. In this case the p_x state constitutes the lowest excited state followed by the p_y and the p_z state. As the platelet thickness is very small, the p_z state is expected at very high energies. A similar reasoning applies to the excited hole states. Figure 1(b) provides an overview of the lowest allowed optical transitions: The ground state transition occurs between the electron and hole s states, the first excited state transition is related to the lowest p states, which we label p_x, as the x axis corresponds to the longest platelet dimension.

The electronic properties and optical transitions of our 4.5 ML CdSe NPLs are calculated in accordance with TEM data (see SM [9]). Following our previous work [3], the electronic structure is obtained using a 3D implementation of eight-band $\mathbf{k} \cdot \mathbf{p}$ envelope function theory. The Coulomb interaction is taken into account via a Hartree self-consistency cycle, performed separately for electron and hole ground state and their first excited states. Both the effects arising from the dielectric environment and the electron and hole self-energy are included. The calculated heavy hole transition energies $E_{\mathrm{GS}}^{(\mathrm{Theo})}$ and energy spacings $\Delta E^{(\mathrm{Theo})}$ [shown in Fig. 2(c)] are compared to experimental values in Table I of the Supplemental Material [9]. The theoretical and experimental values of the energies and spacings show a very good agreement; the calculated transition rates for the GS agree as well with the experimental results; however, there is disagreement for the ES rate (see SM [9]).

In summary, we have shown that CdSe NPLs exhibit not only lowest s-exciton state (GS) related photoluminescence upon continuum excitation, but also excited state luminescence far below GS saturation, evidenced as p-state related. Calculations and time-integrated PL show a strong increase of the ES-GS energy spacing from about 18 to 38 meV with increasing lateral quantization of the exciton wave function. The existence of an LO phonon bottleneck between ES and GS is confirmed by four methods: (1) a rate equation model for the temperature dependence of the emission dynamics, (2) the temporal course of spectrally resolved ES and GS emission at 4 K showing the ES $\rightarrow$ GS filling, (3) the observation of a minimum in the ES/GS emission intensity ratio derived from the decay kinetics, and (4) from the time-integrated PL. The bottleneck is strongly dependent on the detuning of the ES-GS energy spacing to the LO phonon energy of 25.4 meV in CdSe NPLs. We have thus demonstrated that CdSe NPLs are an attractive system allowing us to control not only the exciton energy states by thickness (z direction) but also with lateral size variation the LO-phonon coupling (x, y direction), and this almost independently of each other.

We acknowledge DFG Projects AC290 and WO477, the CHEMREAGENTS program, and IONX-NC4SOL of the Ministero degli Affari Esteri e della Cooperazione Internazionale.

R. S. and A. W. A. contributed equally to this work.

*Current address: Optoelectronic Materials Section, Delft University of Technology, 2628 BL Delft, Netherlands. alexander.achtstein@tu-berlin.de

[1] A. V. Antanovich, A. V. Prudnikau, D. Melnikau, Y. P. Rakovich, A. Chuvilin, U. Woggon, A. W. Achtstein, and M. V. Artemyev, Nanoscale **7**, 8084 (2015).

[2] S. Ithurria, M. D. Tessier, B. Mahler, R. P. S. M. Lobo, B. Dubertret, and A. L. Efros, Nat. Mater. **10**, 936 (2011).

[3] A. W. Achtstein, A. Schliwa, A. Prudnikau, M. Hardzei, M. V. Artemyev, C. Thomsen, and U. Woggon, Nano Lett. **12**, 3151 (2012).

[4] A. Naeem, F. Masia, S. Christodoulou, I. Moreels, P. Borri, and W. Langbein, Phys. Rev. B **91**, 121302 (2015).

[5] E. Cassette, R. D. Pensack, B. Mahler, and G. D. Scholes, Nat. Commun. **6**, 6086 (2015).

[6] J. Q. Grim, S. Christodoulou, F. Di Stasio, R. Krahne, R. Cingolani, L. Manna, and I. Moreels, Nat. Nanotechnol. **9**, 891 (2014).

[7] A. W. Achtstein, A. V. Prudnikau, M. V. Ermolenko, L. I. Gurinovich, S. V. Gaponenko, U. Woggon, A. V. Baranov, M. Y. Leonov, I. D. Rukhlenko, A. V. Fedorov, and M. V. Artemyev, ACS Nano **8**, 7678 (2014).

[8] L. Biadala, F. Liu, M. D. Tessier, D. R. Yakovlev, B. Dubertret, and M. Bayer, Nano Lett. **14**, 1134 (2014).

[9] See Supplemental Material at http://link.aps.org/supplemental/10.1103/PhysRevLett.116.116802, which includes Refs. [10–23], for details about the rate equation model solution, sample characterization, a results table and details on modeling and experimental analysis.

[10] C. She, I. Fedin, D. S. Dolzhnikov, A. Demortière, R. D. Schaller, M. Pelton, and D. V. Talapin, Nano Lett. **14**, 2772 (2014).

[11] B. Guzelturk, O. Erdem, M. Olutas, Y. Kelestemur, and H. V. Demir, ACS Nano **8**, 12524 (2014).
[12] A. W. Achtstein, A. Antanovich, A. Prudnikau, R. Scott, U. Woggon, and M. Artemyev, J. Phys. Chem. C **119**, 20156 (2015).
[13] B. Yuma, S. Berciaud, J. Besbas, J. Shaver, S. Santos, S. Ghosh, R. B. Weisman, L. Cognet, M. Gallart, M. Ziegler, B. Hönerlage, B. Lounis, and P. Gilliot, Phys. Rev. B **87**, 205412 (2013).
[14] P. P. Jha and P. Guyot-Sionnest, ACS Nano **3**, 1011 (2009).
[15] P. Sippel, W. Albrecht, J. C. van der Bok, R. J. A. Van Dijk-Moes, T. Hannappel, R. Eichberger, and D. Vanmaekelbergh, Nano Lett. **15**, 2409 (2015).
[16] R. Scott, A. W. Achtstein, A. Prudnikau, A. Antanovich, S. Christodoulou, I. Moreels, M. Artemyev, and U. Woggon, Nano Lett. **15**, 4985 (2015).
[17] R. Benchamekh, N. A. Gippius, J. Even, M. O. Nestoklon, J.-M. Jancu, S. Ithurria, B. Dubertret, A. L. Efros, and P. Voisin, Phys. Rev. B **89**, 035307 (2014).
[18] F. Ferreira de Sousa, S. G. C. Moreira, J. dos Santos da Silva, J. Del Nero, and P. Alcantara, J. Bionanosci. **3**, 1 (2010).
[19] E. B. Ituen, J. E. Asuquo, and O. R. Ogede, Int. J. Comput. Theor. Chem. **2**, 14 (2014).
[20] S.-H. Wei and A. Zunger, Phys. Rev. B **60**, 5404 (1999).
[21] W. Shan, J. J. Song, H. Luo, and J. K. Furdyna, Phys. Rev. B **50**, 8012 (1994).
[22] M. Willatzen and M. Cardona, Phys. Rev. B **51**, 16338 (1995).
[23] Y. D. Kim, M. V. Klein, S. F. Ren, Y. C. Chang, H. Luo, N. Samarth, and J. K. Furdyna, Phys. Rev. B **49**, 7262 (1994).
[24] S. A. Cherevkov, A. V. Fedorov, M. V. Artemyev, A. V. Prudnikau, and A. V. Baranov, Phys. Rev. B **88**, 041303 (2013).
[25] O. Labeau, P. Tamarat, and B. Lounis, Phys. Rev. Lett. **90**, 257404 (2003).
[26] J. Feldmann, G. Peter, E. O. Göbel, P. Dawson, K. Moore, C. Foxon, and R. J. Elliott, Phys. Rev. Lett. **59**, 2337 (1987).
[27] D. J. Norris and M. G. Bawendi, Phys. Rev. B **53**, 16338 (1996).
[28] I. Moreels, G. Rainò, R. Gomes, Z. Hens, T. Stöferle, and R. F. Mahrt, ACS Nano **5**, 8033 (2011).